Environmental Science & Technology

pubs.acs.org/est

Article

United States Influenza 2022–2023 Season Characteristics as Inferred from Wastewater Solids, Influenza Hospitalization, and Syndromic Data

Mary E. Schoen,* Amanda L. Bidwell, Marlene K. Wolfe, and Alexandria B. Boehm

Cite This: *Environ. Sci. Technol.* 2023, 57, 20542–20550

Read Online

ACCESS | Metrics & More | Article Recommendations | Supporting Information

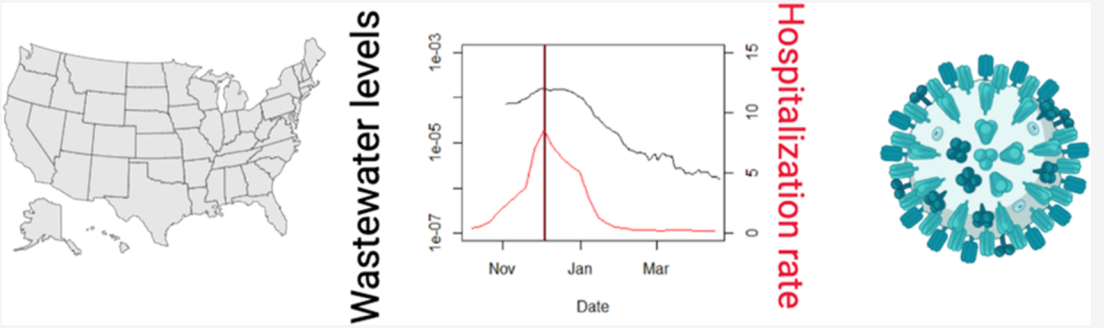

ABSTRACT: Influenza A virus (IAV) causes significant morbidity and mortality in the United States and has pandemic potential. Identifying IAV epidemic patterns is essential to inform the timing of vaccinations and nonpharmaceutical interventions. In a prospective, longitudinal study design, we measured IAV RNA in wastewater settled solids at 163 wastewater treatment plants across 33 states to characterize the 2022–2023 influenza season at the state, health and human services (HHS) regional, and national scales. Influenza season onset, offset, duration, peak, and intensity using IAV RNA in wastewater were compared with those determined using laboratory-confirmed influenza hospitalization rates and outpatient visits for influenza-like illness (ILI). The onset for HHS regions as determined by IAV RNA in wastewater roughly corresponded with those determined using ILI when the annual geometric mean of IAV RNA concentration was used as a baseline (i.e., the threshold that triggers onset), although offsets between the two differed. IAV RNA in wastewater provided early warning of onset, compared to the ILI estimate, when the baseline was set at twice the limit of IAV RNA detection in wastewater. Peak when determined by IAV RNA in wastewater generally preceded peak determined by IAV hospitalization rate by 2 weeks or less. IAV RNA in wastewater settled solids is an IAV-specific indicator that can be used to augment clinical surveillance for seasonal influenza epidemic timing and intensity.

KEYWORDS: *wastewater-based epidemiology, onset, epidemic pattern, baseline, influenza A*

1. INTRODUCTION

Influenza causes significant morbidity and mortality in the United States (US) causing an estimated 44 million illnesses and upward of 41,000 deaths annually and costing $16.3 billion in lost wages and hospitalizations.[1] Influenza can be caused by influenza A and B viruses; however, influenza B infections have been less common in recent years in the US.[2] Influenza vaccines are available annually and reduce the risk of severe illness.[1] However, immune history and antigenic mismatch between the vaccine and circulating strains can modulate vaccine effectiveness.[3] Influenza A virus (IAV) also has pandemic potential, owing to recombination that occurs frequently among influenza A virus (IAV) subtypes. Several subtypes emerged over the past decade that cause severe illness and evaded seasonal vaccines.[4,5]

Understanding the timing and severity of the annual influenza season is essential in guiding public health recommendations and planning for hospital and clinical resources. The US Center for Disease Control and Prevention (CDC) along with researchers characterize the US influenza season by estimating the onset, offset, duration, peak, and intensity (defined in Table 1) using three clinical indicators with historical data: outpatient visits for influenza-like illness (ILI); influenza-related hospitalizations; and influenza- and pneumonia-related deaths.[6−8] These clinical indicators have been used for decades and allow comparison across influenza seasons but have known limitations. For example, ILI can

Received: September 13, 2023
Revised: November 3, 2023
Accepted: November 7, 2023
Published: November 28, 2023

Table 1. Summary of Influenza Season Characteristics, Inputs, and Approach Details[a]

characteristics	description	input	inclusion criteria	approach
onset/offset	day when measure was above/below the baseline value and remained there for at least two additional weeks	Avg_IAV_Region (R1, R4, R5, R8, and R9)	regions with collection between 6/1/2022 and 5/31/2023 with coverage of two or more states	wastewater baseline values were calculated as described in Section 2.2.3; methods 2 and 3 require 11 months of collection; ILI baseline values were obtained from FluView; baseline values were compared to the input time series to identify onset and offset based on conditions in the description
		Avg_IAV_State (AL, CA, CO, FL, GA, IL, KS, MI, NH, and TX)	states with collection between 6/1/2022 and 5/31/2023 with coverage of two or more WWTPs	
		ILI Region (R1, R4, R5, R8, and R9)	regions with available IAV wastewater data	
duration	the number of days between onset and offset	same as onset/offset		
peak/intensity	the date/magnitude of the maximum input value during an influenza season	Avg_IAV_State (CA, CO, GA, MN, MI, and UT)	states with hospitalization data and coverage of two or more WWTPs between 6/1/2022 and 5/31/2023	the maximum of the input time series was identified to characterize peak and intensity
		state hospitalization rate (CA, CO, GA, MN, MI, and UT)	all states for which Avg_IAV_State was calculated	
		Avg_IAV_US	NA	
		overall hospitalization rate	NA	

[a]Inputs were limited to those with sufficient available data for wastewater measurements or clinical measures as explained in the methods. NA: not applicable.

include other respiratory illnesses such as COVID-19 and relies on the care-seeking behaviors of infected individuals. Hospitalizations and deaths reflect severe illness and occur well after initial infections occur. These indicators also have a reporting lag; are reported at large scales, e.g., aggregated by state or US Health and Human Services (HHS) region; and, in the case of hospitalizations, have limited coverage across the US.[6] Recently, wastewater concentrations of IAV RNA have been shown to reflect the occurrence of influenza A in contributing communities.[9] In this study, we investigate how IAV RNA concentrations in wastewater, measured throughout the US in a prospective longitudinal study, can augment clinical indicators to characterize the 2022−2023 influenza season.

To the best of our knowledge, several previous studies have compared IAV RNA in wastewater to influenza occurrence in communities contributing to wastewater. Wolfe et al.[9] determined that IAV RNA was enriched in wastewater solids compared to liquid wastewater and that concentrations correlated with cases identified during active influenza surveillance efforts at two universities. Mercier et al.[10] used IAV concentrations in liquid wastewater and sludge to forecast a municipal IAV outbreak and provide real-time information on the outbreak subtype. Stadler et al.[11] showed that the presence of IAV RNA in liquid wastewater correlated to the presence of IAV at K-12 schools. Boehm et al.[12] showed that IAV RNA in wastewater solids at a large treatment plant serving 1.5 million people correlated with state-aggregated IAV test positivity rates. Lastly, Boehm et al.[13] identified a "tripledemic" when concentrations of IAV, respiratory syncytial virus, and SARS-CoV-2 RNA in wastewater solids peaked simultaneously in the Greater San Francisco Bay Area of California; the wastewater data was used to identify localized onset and offset of wastewater events. These previous studies focused on small geographical areas to inform the IAV activity in local communities; this study examines IAV RNA concentrations in wastewater across the entire US to estimate the timing of the influenza season for states, regions, and the US.

This study compares onset, offset, duration, peak (i.e., date of highest measure), and intensity (i.e., value at time of peak) of the 2022−2023 influenza season using clinical data and IAV RNA concentrations in wastewater settled solids aggregated to match the spatial scales over which clinical data are typically aggregated. Influenza season characteristics are then estimated on a smaller scale using IAV concentrations to illustrate the progression of onset.

2. METHODS

2.1. Input Data. *2.1.1. Clinical Data.* Influenza hospitalization rates (hereafter hospitalization rates) are calculated as the number of residents of a defined area who are hospitalized with a positive influenza laboratory test divided by the population within the area. State hospitalization rates are calculated and reported by the Influenza Hospitalization Surveillance Network (FluSurv-NET), a collaboration between the CDC, the Emerging Infections Program Network, and state and local health departments in 13 geographically distributed areas in the US that conduct population-based surveillance. Cases are identified from hospital, laboratory, and admission databases and infection control logs for patients with a documented positive influenza test (i.e., viral culture, direct/indirect fluorescent antibody assay, reverse transcription-

https://doi.org/10.1021/acs.est.3c07526
Environ. Sci. Technol. 2023, 57, 20542−20550

polymerase chain reaction (RT-PCR), or a rapid influenza diagnostic test).[14] Hospitalization rates are reported on a weekly basis, anchored to the Saturday marking the end of each week and organized by influenza season. Hospitalization rates in units of hospitalizations per 100,000 population were downloaded from FluSurv-NET for all available states for the 2022−2023 influenza season including CA, CO, CT, GA, MD, MI, NM, NY, OH, OR, TN, and UT along with an overall network rate (herein referred to as the overall hospitalization rate).

The US Outpatient Influenza-like Illness Surveillance Network (ILINet) collects information on outpatient visits from 2000 outpatient healthcare providers in all 50 states for respiratory illness.[15] ILINet captures visits due to any respiratory pathogen that presents with the symptoms of fever and cough or sore throat. The percentage of patient visits to healthcare providers for ILI is reported on a weekly basis, anchored to the Saturday marking the end of each week, through the online FluView Interactive platform for the US, HHS regions, and states.[2]

To identify onset and offset, CDC calculates an ILI baseline value during nonflu weeks for HHS regions 1−10 (HHS region map available in FluView Interactive[2]) and the US. The baselines are developed by calculating the mean ILI during noninfluenza weeks for the most recent three seasons excluding the COVID-19 pandemic and adding two standard deviations.[15] We viewed the baseline values along with the time series of ILI for HHS regions in FluView Interactive.

2.1.2. IAV RNA in Wastewater Solids. Samples were collected typically three times per week at up to 163 wastewater treatment plants (WWTPs) between January 5, 2022, and May 31, 2023 (Figure S1 and Table S1). Maximum sampling frequency was daily at 8 CA WWTPs. The date on which WWTPs started participating in the monitoring effort varied between January 5, 2022, and May 24, 2023 (Table S1).

Composite samples of settled solids were collected from the primary clarifier, or solids were obtained from composited raw influent by either using an Imhoff cone,[16] or allowing the influent to settle for 10−15 min, and using a serological pipet to aspirate the settled solids into a falcon tube (Table S1). Previous work suggests no identifiable differences between solid collection methods,[19] and no attempt to account for the different approaches of obtaining solids was made in the present study. Samples were collected by WWTP staff and sent at 4 °C to the laboratory where they were processed immediately. The time between sample collection and receipt at the lab was typically between 1 and 3 days; during this time, limited degradation of the RNA targets is expected.[17,18] Table S1 provides additional information on the WWTPs including the type of sample, the populations served, and the number of samples collected. In total, these WWTPs serve 11.6% of the US population. A total of 18,590 samples were collected and analyzed.

Wastewater solids were subjected to preanalytical processing to obtain nucleic acid extracts as reported in detail in a number of different publications[12,19,20] and on protocols.io[20] and outlined briefly in the Supporting Information (SI). Bovine coronavirus (BCoV) vaccine was spiked into each sample to gain insight into nucleic acid recovery. The nucleic acids were then used as templates in droplet digital RT-PCR reactions to measure concentrations of the IAV M1 gene,[21] pepper mild mottle virus (PMMoV) RNA,[21] and BCoV RNA.[21] No additional sequencing or targeted RT-qPCR for IAV typing was conducted to verify that the IAV was human-related; cross-reactivity of the detection methods with animal influenza viruses is possible. The IAV assay was multiplexed with other assays, and those assays changed over the period of the project as public health needs changed and new research to support the monitoring of additional disease targets became available; the assays with which IAV was multiplexed are provided in Figure S2. The analytical approaches including the thresholding of the fluorescent values from the instrument are described in detail in the data descriptor by Boehm et al.[21] and are not repeated here. Concentrations are reported in units of copies per gram of dry weight (cp/g). Positive and negative extraction and RT-PCR controls were run alongside all samples, as described elsewhere[21] and in the SI. These data have not been previously published aside from samples collected between 7/1/22 and 5/7/23 at eight of the 163 WWTPs in this study, all located in the greater San Francisco Bay Area of California.[13]

2.2. Data Analysis. *2.2.1. Aggregated IAV/PMMoV.* We aggregated the wastewater data across WWTPs to calculate daily average concentrations of IAV RNA normalized by PMMoV RNA for states and HHS regions. PMMoV normalization was done to account for potential differential recoveries of viral nucleic acids during the preanalytical steps,[22] and because a mass balance model suggests that IAV/PMMoV should scale as disease incidence rate.[23] The Avg_IAV_State_d or Avg_IAV_Region_d is the population-weighted average of $\text{IAV/PMMoV}_{n,d}$ on day d from N WWTPs contributing to the state or region calculated as

$$\text{Avg\_IAV\_State}_d \text{ or } \text{Avg\_IAV\_Region}_d = \frac{\sum_{n=1}^{N} \text{pop}_n \times \text{IAV/PMMoV}_{n,d}}{\sum_{n=1}^{N} \text{pop}_n} \quad (1)$$

where pop_n is the population served by WWTP n and $\text{IAV/PMMoV}_{n,d}$ is the five-sample trimmed average of IAV/PMMoV from plant n on day d. Prior to calculating the aggregated line, nondetect values are set to the limit of detection of 500 cp/g normalized by the average PMMoV value for the WWTP. For days when a WWTP did not have a sample, $\text{IAV/PMMoV}_{n,d}$ was estimated using linear interpolation between adjacent values. Weekly median Avg_IAV_State or Avg_IAV_Region was calculated (Sunday through Saturday) for comparison with the hospitalization rate.

We aggregated the average concentrations across states to calculate daily average concentration of IAV/PMMoV for the US. The Avg_IAV_US_d is the population-weighted average of $\text{Avg\_IAV\_State}_{s,d}$ on day d from s states calculated as

$$\text{Avg\_IAV\_US}_d = \frac{\sum_{s=1}^{S} \text{pop}_s \times \text{Avg\_IAV\_State}_{s,d}}{\sum_{s=1}^{S} \text{pop}_s} \quad (2)$$

where pop_s is the population of state s and $\text{Avg\_IAV\_State}_{s,d}$ is calculated for state s using eq 1. We aggregated over states, as opposed to WWTPs, to avoid oversampling of states with many participating WWTPs. Only states with coverage of two or more WWTPs at time of analysis were included in eq 2 (i.e., AL, CA, CO, FL, GA, ID, IL, IN, IA, KS, ME, MD, MI, MN, NH, NJ, NC, OH, PA, TX, UT, VT, and VA). Weekly median Avg_IAV_US_d was calculated (Sunday through Saturday) for comparison with the overall hospitalization rate.

https://doi.org/10.1021/acs.est.3c07526
Environ. Sci. Technol. 2023, 57, 20542−20550

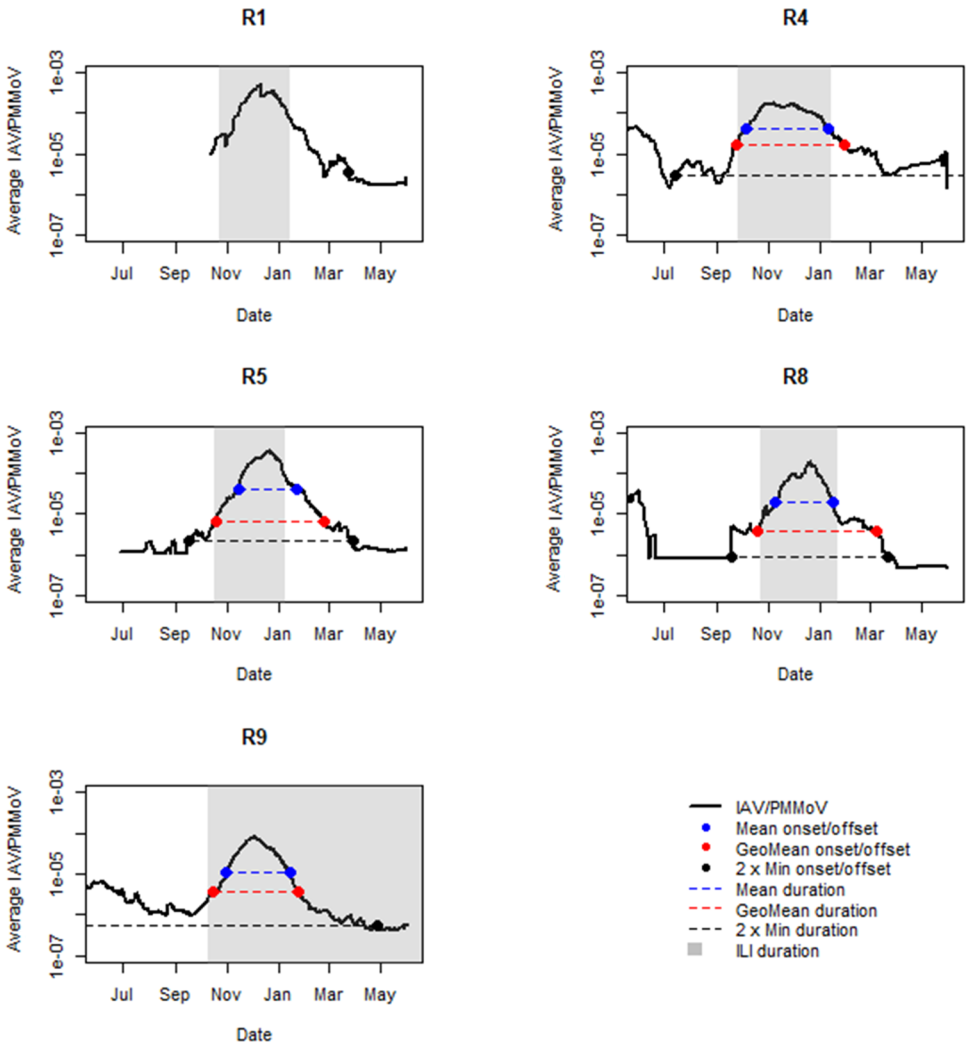

Figure 1. Comparison of alternative baseline Avg_IAV_Region values (*y*-axis) and corresponding influenza season onset, offset, and duration for HHS regions (abbreviated R in title) for 2022−2023 influenza season (*x*-axis). Baseline values were calculated using Avg_IAV_Region annual mean (Mean), annual geometric mean (GeoMean), and twice the minimum observation (2 × Min). Shading indicates ILI onset, offset, and duration. Lines or shading that extend beyond the plotted time period indicate that onset or offset did not occur during the period of analysis using the selected baseline. Missing duration lines and onset/offset points indicate that data was not available for calculation.

2.2.2. Influenza Season Characteristics. Table 1 summarizes the approaches used to estimate the influenza season characteristics of the onset, offset, duration, peak, and intensity for each data input. Influenza surveillance by CDC begins 10/2/2022 and ends 9/30/2023 for the 2022−2023 season, whereas the period of analysis for this paper was 6/1/2022−5/31/2023 to capture the onset in states and regions that occurred earlier than the CDC starting date of 10/2/2022.

For analysis of peak and intensity, we compared characteristics using wastewater to those using hospitalization rates, given that the hospitalization rates are specific to influenza A infections. The comparison was limited to the FluSurv-NET reporting spatial scales of state and the overall network estimate (listed in Table 1). For analysis of onset, offset, and duration, we compared characteristics using wastewater to those using ILI, given that ILI is used by CDC to inform these characteristics.[15] The comparison was limited to the ILI reporting scale of the HHS region (listed in Table 1). Onset, offset, and duration were also estimated for states using wastewater data.

2.2.3. Calculation of Baseline Using Wastewater IAV/PMMoV. Mirroring the approaches used by CDC and other researchers in defining influenza season onset using an off-season baseline value,[24] we calculated wastewater baseline values using four different approaches: (1) recording the Avg_IAV_Region values that correspond with the ILI onset and offset dates, (2) calculating the annual Avg_IAV_Region mean over of the period of analysis, (3) calculating the annual Avg_IAV_Region geometric mean over the period of analysis, and (4) calculating twice the minimum Avg_IAV_Region from start of collection (which varied) to the end of the period of analysis (representing roughly twice the lowest detectable concentration). Method 1 is dependent on ILI and interprets the ILI baseline in terms of Avg_IAV_Region. Methods 2 and 3 are based on WHO guidance for the aggregate average method,[25] but using one year of data rather than multiple years (as multiple years were not available), while method 4 does not require a full year of observation. The rationale for method 4 was that during periods devoid of influenza activity, concentrations of IAV RNA in wastewater tend to be nondetect.[13] State baseline values were estimated using

https://doi.org/10.1021/acs.est.3c07526
Environ. Sci. Technol. 2023, 57, 20542−20550

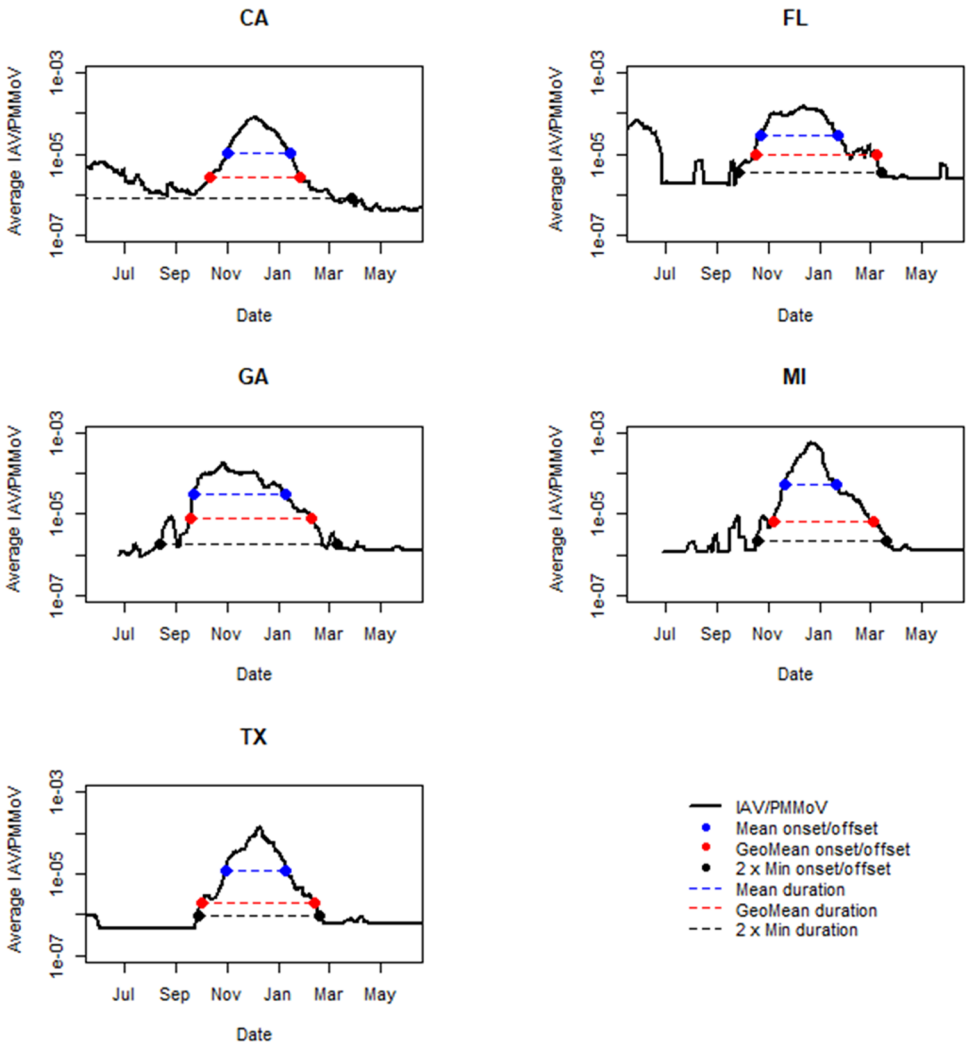

Figure 2. Comparison of alternative baseline Avg_IAV_State values (*y*-axis) and corresponding influenza season onset, offset, and duration for states with at least 11 months of data for 2022−2023 influenza season (*x*-axis). Baseline values were calculated using Avg_IAV_State annual mean (Mean), annual geometric mean (GeoMean), and twice the minimum observation (2 × Min). Lines that extend beyond the plotted time period indicate that onset or offset did not occur during the period of analysis using the selected baseline.

Avg_IAV_State data and methods 2−4; ILI baseline values are not available at the state level.

2.2.4. Additional Analysis. Cumulative empirical curves of the proportion of states with onset during the 2022−2023 influenza season were generated using wastewater IAV baselines calculated by methods 2, 3, and 4. Linear relationships were evaluated between $\log_{10}$ transformed (a) weekly median Avg_IAV_State and hospitalization rate at the state level and (b) weekly median Avg_IAV_US and overall hospitalization rate (details provided in SI).

3. RESULTS

3.1. QA/QC. The positive and negative controls were positive and negative, respectfully indicating no contamination. The median BCoV recovery across all of the samples was 1.21 (interquartile range = 0.84−1.42) suggesting reasonable recovery; recovery values greater than 1 are likely a result of uncertainties associated with quantifying the quantity spiked into the samples. The reporting table from the Environmental Microbiology Minimal Information (EMMI) guidelines has been provided previously in Boehm et al.[21] Previous work indicated minimal inhibition of the IAV assay using the applied preanalytical and analytical approaches.[21]

3.2. IAV Wastewater Data. Wastewater IAV concentrations collected from 163 WWTPs covering 33 states ranged between below the limit of detection and 15,438,760 cp/g over the period of analysis of 6/1/2022−5/31/2023 (Figure S3 and Table S1). The IAV concentrations were normalized by PMMoV (Figure S4) and aggregated to calculate the state and HHS regional average concentrations (i.e., Avg_IAV_State and Avg_IAV_Region). The WWTP, state, and HHS regional wastewater concentrations followed seasonal patterns over the period of analysis with elevated concentrations in the winter season compared to summer but also indicated sporadic increases in concentrations throughout the summer of the 2021−2022 season (e.g., Figures S3, S4, 1, and 2).

3.3. IAV Baseline Values. To identify the onset and offset of influenza season using wastewater, we calculated baseline values of Avg_IAV_State or Avg_IAV_Region using concentrations corresponding to ILI onset and offset (method 1), the annual mean (method 2), the annual geometric mean (method 3), and twice the minimum (method 4) (Figure 1 and Table S2 for HHS regions, Figure 2 and Table S3 for states). Across

https://doi.org/10.1021/acs.est.3c07526
Environ. Sci. Technol. 2023, 57, 20542−20550

states and HHS regions, the lowest wastewater baselines were those defined as twice the minimum (range of 5.70×10^{-7}–3.46×10^{-6} across HHS regions and 8.10×10^{-7}–3.54×10^{-6} across states) while the highest baselines were those defined as the annual mean (range of 1.06×10^{-5}–4.14×10^{-5} across HHS regions and 1.02×10^{-5}–5.12×10^{-5} across states), with the exception of HHS region 5 (R5) for which the baseline corresponding to the ILI offset was higher than the annual mean baseline. Baselines defined as the annual geometric mean and corresponding to the ILI onset and offset (only applicable to HHS regions) were generally between those described above.

3.4. Onset, Offset, and Duration. *3.4.1. HHS Region Comparison.* The onset, offset, and durations of the 2022–2023 influenza season determined using the ILI baseline and wastewater baseline values using methods 2–4 are compared in Figure 1 and Table S4 for HHS regions. Onset was earliest in R4 (Southeast) followed by R9 (West), R5 (Midwest) or R8 (Central), and R1 (Northeast) for all baseline approaches. Note that we did not have sufficient data to examine onsets in the other HHS regions.

Comparing onset determined using ILI and wastewater, onset using the Avg_IAV_Region baseline corresponding to twice the minimum was up to 85 days earlier than onset calculated by the other approaches (range of 30–85 days); whereas, the ILI, Avg_IAV_Region annual mean, and Avg_IAV_Region annual geometric mean onset values differed less than 30 days across the HHS regions. Onset determined by the Avg_IAV_Region annual mean was the latest across approaches. Onset for R9 could not be determined using the baseline corresponding to twice the minimum because observations remained elevated throughout all of 2022.

The offset for HHS regions based on the Avg_IAV_Region annual mean baseline fell within a 14-day range (range of 1/8/2023–1/22/2023). The ILI offset occurred during the same 14-day range, with the exception of R9 which did not reach an offset by the end of the analysis (5/31/2023) with ILI levels just above the baseline for many weeks (data now shown). The offset using baselines of the Avg_IAV_Region geometric mean and twice the minimum generally occurred within a wider date range (between 1/24/2023 and 4/28/2023). As a result, the influenza season durations were greater using these two approaches rather than the ILI baseline or Avg_IAV_Region annual mean baseline (with the exception of R9).

3.4.2. State Estimates. State-level onset, offset, and duration were calculated using Avg_IAV_State annual mean, annual geometric mean, and twice the minimum (Figure 2 and Table S5). The order of onset and offset by method using state data mirrored the HHS regional analysis as did the comparison of the duration. Similar to the regional analysis, onset for CA (in R9) could not be determined using the baseline corresponding to twice the minimum because observations remained elevated throughout the period of analysis.

Cumulative curves of the proportion of states achieving onset over time during the 2022–2023 influenza season are compared using baselines of Avg_IAV_State annual mean (five states with annual data), annual geometric mean (five states with annual data), or twice the minimum (nine states with data) (Figure 3). The curves using the baselines of annual geometric mean and annual mean were shifted right compared to the curve using twice the minimum, consistent with the later onset illustrated in Figure 2.

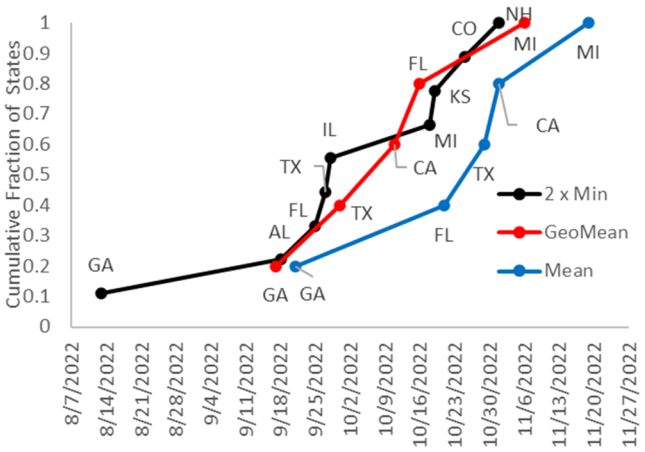

Figure 3. Cumulative curves of the proportion of states with onset (*y*-axis) over time (*x*-axis) during the 2022–2023 influenza season using Avg_IAV_State baselines of the annual mean ($N = 5$), geometric mean ($N = 5$), or twice the minimum observation ($2 \times$ Min) ($N = 9$).

The curve using the Avg_IAV_State baseline of twice the minimum was roughly sigmoidal, indicating that the onset happened over a narrow time interval for the majority of states despite the earliest onset in GA. GA preceded other states by 36, 30, and 13 days using baselines of twice the minimum, annual geometric mean, and annual mean, respectively. The limited number of states with sufficient data for the mean and geometric mean baselines made it difficult to assess the curve shape. The trajectory of onset moved outward from the origin in the Southeast when using all of the selected baselines. However, the order of onset varied by the baseline method; e.g., onset in FL occurred before TX using the annual mean and twice the minimum baselines but after using the annual geometric mean baseline.

3.5. Peak and Intensity. *3.5.1. State Comparison.* The 2022–2023 influenza season state peaks (i.e., date of highest measure) and intensities (i.e., value at time of peak) are compared using wastewater (Avg_IAV_State) and laboratory-confirmed influenza hospitalizations (hospitalization rate) in Figure S5 and Table S6. The Avg_IAV_State peaks generally preceded the hospitalization rate peaks (range of 2–12 days), with the exception of MN. When the intensity as measured by hospitalization rate increased across states, the intensity measured by Avg_IAV_State also increased across states (Table S6). The Avg_IAV_State peak values were roughly 2 orders of magnitude greater than the Avg_IAV_State baseline values calculated using twice the minimum observation and between roughly 1 and 2 orders of magnitude greater than the Avg_IAV_State annual mean or annual geometric mean baselines.

3.5.2. US Comparison. When Avg_IAV_State was aggregated to create a population-weighted US value, the peaks estimated using the Avg_IAV_US and overall hospitalization rate fall 1 day apart (Figure 4, 12/03/2022 and 12/04/2022) despite representing different states (Figures S6 and S7). Avg_IAV_US did not cover states with the highest intensities, as measured by hospitalization rate (e.g., CT, NM, NY, OR, and TN). FluServe-Net did not include 17 states covered by Avg_IAV_US, particularly those with early season onset (e.g., FL and TX).

3.5.3. Linear Relationship. We found a significant relationship between $\log_{10}$ Avg_IAV_State (expressed as the median

https://doi.org/10.1021/acs.est.3c07526
Environ. Sci. Technol. 2023, 57, 20542–20550

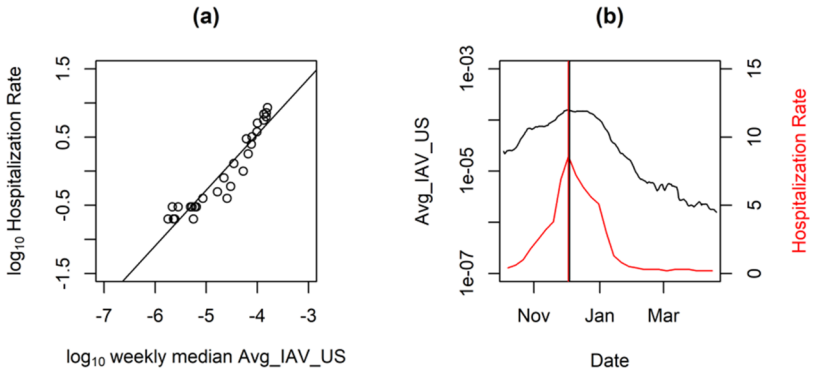

Figure 4. 2022−2023 Overall FluServe-Net hospitalization rate (hospitalizations per 100,000 population) and Avg_IAV_US: (a) linear relationship using $\log_{10}$ transformed values and weekly median Avg_IAV_US and (b) comparison of peak and intensity with vertical lines presenting time of peak.

of daily values each week) and $\log_{10}$ hospitalization rate (reported weekly) for each state ($p < 0.001$, R^2 range of 0.74−0.90 across states) (Figure S8 and Table S7). We also found a significant relationship between $\log_{10}$ Avg_IAV_US (expressed as the median of daily values each week) and $\log_{10}$ overall hospitalization rate (reported weekly) ($p < 0.001$, R^2 of 0.89) (Figure 4 and Table S7).

4. DISCUSSION

We used information on IAV and PMMoV RNA targets in municipal wastewater solids to estimate the 2022−2023 influenza season onset, offset, duration, peak, and intensity. The CDC and other agencies use clinical data to estimate these characteristics.[6−8] To compare the wastewater estimates to the clinical estimates, we aggregated the data from 163 WWTPs in 33 states to represent scales typically used for clinical data (e.g., state, HHS region, or national). Then, we estimated baseline concentrations of the aggregated wastewater data using approaches similar to those originally proposed for clinical data, but with one year of data (or less) rather than multiple years.[25]

The wastewater baseline values were determined individually for HHS regions and states, as the ILI baseline values used by the CDC are unique to each HHS region. The range of wastewater baseline values across the 5 regions covered approximately 1 $\log_{10}$ when set to correspond with ILI onset (minimum of 2.31×10^{-6} and maximum of 2.73×10^{-5}). In comparison, the ranges of wastewater baseline values for HHS regions and states determined independently of ILI (baseline methods 2−4) covered less than 0.8 $\log_{10}$. The wastewater baseline values set to twice the minimum ranged between 5.70×10^{-7} and 3.46×10^{-6} across HHS regions and 8.1×10^{-7} and 3.54×10^{-6} across states. For reference, the difference between intensity and baseline using twice the minimum for each state was 2 $\log_{10}$ or greater. Future work can explore whether baseline values are applicable across states and/or spatial scales.

Regional results indicated that onset determined using wastewater and a baseline of the annual geometric mean was similar to the onset estimated using the ILI baseline; whereas, onset determined using wastewater and a baseline of the annual mean was later than ILI-estimated onsets. Using twice the minimum observation as wastewater baseline provided an early warning (between 30 and 75 days) compared to ILI-estimated onset. We applied the same approaches to estimate wastewater baseline values for states for which ILI baseline data are not available. The pattern of onset across baseline methods mirrored the regional analysis; in addition, the baseline method influenced the estimated progression across states in terms of the order of onset. Thus, for the 2022−2023 influenza season, the selection of baseline using wastewater data influenced the interpretation of onset in time and across space.

Characterizing the differences between baseline methods allows public health officials to select a baseline that best matches their goals for identification and communication about influenza season. For a wastewater baseline that aligns with expected increases in ILI, the geometric mean is best, as the onset of regions using the geometric mean of wastewater data aligns with the ILI-estimated onset. Alternatively, early warning of season onset may be desirable for public health decision making, in which case, a baseline based on the minimum observation may be useful. However, selecting the minimum threshold is challenging given variation of IAV in municipal wastewater solids within each season (as illustrated by HHS R9 in Figure 1 for which summertime influenza activity interfered with identifying typical influenza season onset) and unknown variation between seasons (data not available to characterize). For example, IAV inputs from infected birds or wildlife could temporarily increase the wastewater concentration for wastewater treatment and collection systems vulnerable to nonhuman inputs. The wastewater threshold for identifying onset and offset should be set high enough to be higher than the random variation and noise in the IAV in municipal wastewater solids during the off-season.

Using the value of twice the minimal observation to identify IAV onset is similar to the approach applied by Boehm et al.[13] for identifying influenza wastewater events at individual WWTPs. In the present study, this baseline method seemed to capture the entire periods of increasing and decreasing concentrations in wastewater during the seasonal IAV epidemic. However, in California, spatially aggregated wastewater levels remained above this baseline for the entire summer prior to the winter influenza season. California experienced higher than normal summertime influenza activity in 2022 after not having influenza during the height of the COVID-19 pandemic as illustrated by the hospitalization rate and ILI data in FluView Interactive,[14,15] which may have contributed to the high levels in wastewater in summer 2022. Choosing a slightly higher value (3 times the minimum) as a

https://doi.org/10.1021/acs.est.3c07526
Environ. Sci. Technol. 2023, 57, 20542−20550

baseline for California would have led to an offset in September, followed closely by onset.

The definition of the onset is also important from a practical perspective. We adopted the description of ILI and wastewater onset date used by the CDC which identifies the date as that after which the baseline is exceeded for two consecutive weeks. This definition precludes real-time determination of onset as it requires a 2-week period of data, which would retroactively identify an onset date at the beginning of the period when used in real time. Alternatively, a look-back window could be implemented, as applied by Boehm et al.[13] for IAV, which provides real-time estimation of an onset date assigned to the end of a 2-week period of data. Further work could investigate that definition.

We also compared the peak and intensity of the 2022−2023 influenza season using influenza hospitalization rates to that using wastewater data for states and the US. We found that the peaks estimated by wastewater data generally preceded the peaks determined by hospitalization rates for states by 2−14 days. The earlier peak is not surprising given that the wastewater data capture viral shedding from both asymptomatic and symptomatic infections as well as from mild and severe infections, whereas the hospitalization rate captures the most severe cases. The general agreement of the peak combined with the strong relationship between aggregated wastewater data and hospitalization rate suggests one could use IAV RNA in wastewater solids as an early warning for identifying peak hospitalization, especially for states with limited formal clinical surveillance. The wastewater data could also be used at more localized scales to identify peak events, as has been illustrated previously at the building,[11] subsewershed,[9] and sewershed[13] levels.

A strength of the wastewater data used in this analysis is the wide coverage of WWTPs across the US. This allows analysis at a localized scale, as exemplified here by the onset analysis at the state scale and at the sewershed level elsewhere.[13] This analysis is enabled by the ability to aggregate information from individual WWTPs, which is possible due to the consistent methods applied to obtain IAV and PMMoV RNA concentrations across locations. Another strength is that the wastewater data captures IAV-specific mild illness and asymptomatic illness and is agnostic as to whether individuals seek medical care; whereas, the ILI data captures data from individuals with various respiratory illnesses seeking medical care, which resulted in the exclusion of the ILI data collected over the pandemic in the calculation of the baseline.[15] This is particularly important as COVID-19 surveillance is expected to transition to a model that is more similar to influenza surveillance, and there is a need to distinguish between IAV and COVID-19 outbreaks that share similar ailments and symptoms.

Limitations of using wastewater data to characterize influenza season include the fact that wastewater data cannot be disaggregated by age of population, vaccine status of population, or severity of disease. WWTPs participation is voluntary; therefore, coverage may vary over time, and sample sites are not based on a strategic sampling plan to provide optimal coverage across the US, regions, or states. The method used herein to quantify IAV in wastewater is not human-specific and may enumerate IAV from other sources, such as birds, wildlife, and domesticated animals; however, this limitation could be addressed in future work using animal-specific molecular source tracking tools. Additionally, the wastewater data lack the historical record that clinical data provide.

Wastewater settled solids data represent an additional surveillance indicator of influenza that can be used to characterize the influenza season along with clinical data across scales currently unavailable using clinical data (e.g., US down to sewershed). While the rates of influenza-associated hospitalizations are a product of the transmissibility and the clinical severity of influenza,[7] wastewater data may be considered as a proxy to transmissibility, similar to ILI, but IAV-specific. As additional data are collected over multiple influenza seasons, the approaches introduced in this work can be refined to better capture the variation in IAV and PMMoV targets in municipal wastewater solids across seasons and further analysis can be conducted such as the moving epidemic method or aggregate average method[25] to evaluate IAV onset and severity.[7]

■ ASSOCIATED CONTENT

Data Availability Statement

Wastewater data are publicly available at the Stanford Digital Repository: 10.25740/mf441vr6745.

Supporting Information

The Supporting Information is available free of charge at https://pubs.acs.org/doi/10.1021/acs.est.3c07526.

QA/QC methods, raw data, HHS regions, baseline values, and the relationship between wastewater data and hospitalization rate (PDF)

■ AUTHOR INFORMATION

Corresponding Author

Mary E. Schoen − *Soller Environmental, LLC, Berkeley, California 94703, United States;* orcid.org/0000-0002-2837-3517; Email: mschoen@sollerenvironmental.com

Authors

Amanda L. Bidwell − *Department of Civil & Environmental Engineering, School of Engineering and Doerr School of Sustainability, Stanford University, Stanford, California 94305, United States*

Marlene K. Wolfe − *Gangarosa Department of Environmental Health, Rollins School of Public Health, Emory University, Atlanta, Georgia 30322, United States;* orcid.org/0000-0002-6476-0450

Alexandria B. Boehm − *Department of Civil & Environmental Engineering, School of Engineering and Doerr 8 School of Sustainability, Stanford University, Stanford, California 94305, United States;* orcid.org/0000-0002-8162-5090

Complete contact information is available at: https://pubs.acs.org/10.1021/acs.est.3c07526

Author Contributions

The manuscript was written through contributions of all authors. All authors have given approval to the final version of the manuscript. M.E.S. and A.L.B.: computation; M.E.S. and A.B.B.: writing; M.E.S., A.L.B., M.K.W., and A.B.B.: conception and editing of this article.

Funding

This work was supported by gifts from the CDC Foundation and the Sergey Brin Family Foundation to A.B.B.

Notes

The authors declare no competing financial interest.

■ ACKNOWLEDGMENTS

The authors acknowledge the numerous people who contributed to wastewater sample collection. The GA was created using Biorender.com.

■ REFERENCES

(1) Molinari, N.-A. M.; Ortega-Sanchez, I. R.; Messonnier, M. L.; Thompson, W. W.; Wortley, P. M.; Weintraub, E.; Bridges, C. B. The Annual Impact of Seasonal Influenza in the US: Measuring Disease Burden and Costs. *Vaccine* **2007**, *25* (27), 5086−5096.

(2) Centers for Disease Control and Prevention. FluView Interactive/CDC. https://www.cdc.gov/flu/weekly/fluviewinteractive.htm (accessed Aug 23, 2023).

(3) Lewnard, J. A.; Cobey, S. Immune History and Influenza Vaccine Effectiveness. *Vaccines* **2018**, *6* (2), No. 28, DOI: 10.3390/vaccines6020028.

(4) Yamaji, R.; Saad, M. D.; Davis, C. T.; Swayne, D. E.; Wang, D.; Wong, F. Y. K.; McCauley, J. W.; Peiris, J. S. M.; Webby, R. J.; Fouchier, R. A. M.; Kawaoka, Y.; Zhang, W. Pandemic Potential of Highly Pathogenic Avian Influenza Clade 2.3.4.4 A(H5) Viruses. *Rev. Med. Virol.* **2020**, *30* (3), No. e2099.

(5) Yen, H.-L.; Webster, R. G. Pandemic Influenza as a Current Threat. In *Vaccines for Pandemic Influenza*; Compans, R. W.; Orenstein, W. A., Eds.; Current Topics in Microbiology and Immunology; Springer: Berlin, Heidelberg, 2009; pp 3−24.

(6) U.S. Influenza Surveillance: Purpose and Methods|CDC. https://www.cdc.gov/flu/weekly/overview.htm (accessed Aug 23, 2023).

(7) Biggerstaff, M.; Kniss, K.; Jernigan, D. B.; Brammer, L.; Bresee, J.; Garg, S.; Burns, E.; Reed, C. Systematic Assessment of Multiple Routine and Near Real-Time Indicators to Classify the Severity of Influenza Seasons and Pandemics in the United States, 2003−2004 Through 2015−2016. *Am. J. Epidemiol.* **2018**, *187* (5), 1040−1050.

(8) Biggerstaff, M.; Alper, D.; Dredze, M.; Fox, S.; Fung, I. C.-H.; Hickmann, K. S.; Lewis, B.; Rosenfeld, R.; Shaman, J.; Tsou, M.-H.; Velardi, P.; Vespignani, A.; Finelli, L. for the Influenza Forecasting Contest Working Group. Results from the Centers for Disease Control and Prevention's Predict the 2013−2014 Influenza Season Challenge. *BMC Infect. Dis.* **2016**, *16* (1), No. 357, DOI: 10.1186/s12879-016-1669-x.

(9) Wolfe, M. K.; Duong, D.; Bakker, K. M.; Ammerman, M.; Mortenson, L.; Hughes, B.; Arts, P.; Lauring, A. S.; Fitzsimmons, W. J.; Bendall, E.; Hwang, C. E.; Martin, E. T.; White, B. J.; Boehm, A. B.; Wigginton, K. R. Wastewater-Based Detection of Two Influenza Outbreaks. *Environ. Sci. Technol. Lett.* **2022**, *9* (8), 687−692.

(10) Mercier, E.; D'Aoust, P. M.; Thakali, O.; Hegazy, N.; Jia, J.-J.; Zhang, Z.; Eid, W.; Plaza-Diaz, J.; Kabir, M. P.; Fang, W.; et al. Municipal and Neighbourhood Level Wastewater Surveillance and Subtyping of an Influenza Virus Outbreak. *Sci. Rep.* **2022**, *12* (1), No. 15777.

(11) Wolken, M.; Sun, T.; McCall, C.; Schneider, R.; Caton, K.; Hundley, C.; Hopkins, L.; Ensor, K.; Domakonda, K.; Kalvapalle, P.; Persse, D.; Williams, S.; Stadler, L. B. Wastewater Surveillance of SARS-CoV-2 and Influenza in PreK-12 Schools Shows School, Community, and Citywide Infections. *Water Res.* **2023**, *231*, No. 119648, DOI: 10.1016/j.watres.2023.119648.

(12) Boehm, A. B.; Hughes, B.; Duong, D.; Chan-Herur, V.; Buchman, A.; Wolfe, M. K.; White, B. J. Wastewater Concentrations of Human Influenza, Metapneumovirus, Parainfluenza, Respiratory Syncytial Virus, Rhinovirus, and Seasonal Coronavirus Nucleic-Acids during the COVID-19 Pandemic: A Surveillance Study. *Lancet Microbe* **2023**, *4* (5), e340−e348.

(13) Boehm, A.; Wolfe, M. K.; White, B.; Hughes, B.; Duong, D.; Bidwell, A. *Community Occurrence of Metapneumovirus, Influenza A, and Respiratory Syncytial Virus (RSV) Inferred from Wastewater Solids during the Winter 2022−2023 Tripledemic*; medRxiv, 2023. DOI: 10.1101/2023.06.12.23291120.

(14) Centers for Disease Control and Prevention, National Center for Immunization and Respiratory Diseases (NCIRD). Influenza Hospitalization Surveillance Network (FluSurv-NET). https://gis.cdc.gov/GRASP/Fluview/FluHospRates.html (accessed May 23, 2023).

(15) Centers for Disease Control and Prevention. US Outpatient Influenza-like Illness Surveillance Network (ILINet) https://www.cdc.gov/flu/weekly/overview.htm (accessed May 23, 2023).

(16) AWWA. In *Standard Methods for the Examination of Water and Wastewater*, 21st ed.; Eaton, A. D.; Clesceri, L. S.; Rice, E. W.; Greenberg, A. E., Eds.; American Public Health Association, American Water Works Association, Water Environment Federation: Baltimore, 2005.

(17) Guo, Y.; Li, J.; O'Brien, J.; Sivakumar, M.; Jiang, G. Back-Estimation of Norovirus Infections through Wastewater-Based Epidemiology: A Systematic Review and Parameter Sensitivity. *Water Res.* **2022**, *219*, No. 118610.

(18) Burnet, J.-B.; Cauchie, H.-M.; Walczak, C.; Goeders, N.; Ogorzaly, L. Persistence of Endogenous RNA Biomarkers of SARS-CoV-2 and PMMoV in Raw Wastewater: Impact of Temperature and Implications for Wastewater-Based Epidemiology. *Sci. Total Environ.* **2023**, *857*, No. 159401.

(19) Wolfe, M. K.; Topol, A.; Knudson, A.; Simpson, A.; White, B.; Duc, V.; Yu, A.; Li, L.; Balliet, M.; Stoddard, P.; Han, G.; Wigginton, K. R.; Boehm, A. High-Frequency, High-Throughput Quantification of SARS-CoV-2 RNA in Wastewater Settled Solids at Eight Publicly Owned Treatment Works in Northern California Shows Strong Association with COVID-19 Incidence. *mSystems* **2021**, *6* (5), No. e00829-21.

(20) Topol, A.; Wolfe, M.; Wigginton, K.; White, B.; Boehm, A.*High Throughput RNA Extraction and PCR Inhibitor Removal of Settled Solids for Wastewater Surveillance of SARS-CoV-2 RNA*; protocols.io, 2021. DOI: 10.17504/protocols.io.b2mkqc4w.

(21) Boehm, A. B.; Wolfe, M. K.; Wigginton, K. R.; Bidwell, A.; White, B. J.; Hughes, B.; Duong, D.; Chan-Herur, V.; Bischel, H. N.; Naughton, C. C. Human Viral Nucleic Acids Concentrations in Wastewater Solids from Central and Coastal California USA. *Sci. Data* **2023**, *10* (1), No. 396, DOI: 10.1038/s41597-023-02297-7.

(22) Simpson, A.; Topol, A.; White, B. J.; Wolfe, M. K.; Wigginton, K. R.; Boehm, A. B. Effect of Storage Conditions on SARS-CoV-2 RNA Quantification in Wastewater Solids. *PeerJ* **2021**, *9*, No. e11933.

(23) Wolfe, M. K.; Archana, A.; Catoe, D.; Coffman, M. M.; Dorevich, S.; Graham, K. E.; Kim, S.; Grijalva, L. M.; Roldan-Hernandez, L.; Silverman, A. I.; Sinnott-Armstrong, N.; Vugia, D. J.; Yu, A. T.; Zambrana, W.; Wigginton, K. R.; Boehm, A. B. Scaling of SARS-CoV-2 RNA in Settled Solids from Multiple Wastewater Treatment Plants to Compare Incidence Rates of Laboratory-Confirmed COVID-19 in Their Sewersheds. *Environ. Sci. Technol. Lett.* **2021**, *8* (5), 398−404.

(24) Igboh, L. S.; Roguski, K.; Marcenac, P.; Emukule, G. O.; Charles, M. D.; Tempia, S.; Herring, B.; Vandemaele, K.; Moen, A.; Olsen, S. J.; Wentworth, D. E.; Kondor, R.; Mott, J. A.; Hirve, S.; Bresee, J. S.; Mangtani, P.; Nguipdop-Djomo, P.; Azziz-Baumgartner, E. Timing of Seasonal Influenza Epidemics for 25 Countries in Africa during 2010−19: A Retrospective Analysis. *Lancet Global Health* **2023**, *11* (5), e729−e739.

(25) World Health Organization. *Global Epidemiological Surveillance Standards for Influenza*; World Health Organization: Geneva, 2013 (accessed Dec 01, 2022).